Defense Technical Information Center
Compilation Part Notice

ADP010903

TITLE: Extract Multiple Scaling in Long-Term
Heart Rate Variability

DISTRIBUTION: Approved for public release, distribution unlimited

This paper is part of the following report:

TITLE: Paradigms of Complexity. Fractals and
Structures in the Sciences

To order the complete compilation report, use: ADA392358

The component part is provided here to allow users access to individually authored sections
of proceedings, annals, symposia, ect. However, the component should be considered within
the context of the overall compilation report and not as a stand-alone technical report.

The following component part numbers comprise the compilation report:
ADP010895 thru ADP010929

EXTRACT MULTIPLE SCALING IN LONG-TERM HEART RATE VARIABILITY

D.C. LIN

Department of Mechanical Engineering
Ryerson Polytechnic University
Toronto, Ontario, Canada, M5B 2K3
E-mail: derlin@acs.ryerson.ca

R.L. HUGHSON

Department of Kinesiology
University of Waterloo
Waterloo, Ontario, Canada, N2L 3G1
E-mail: hughson@healthy.uwaterloo.ca

Many natural processes can be characterized by their scale-invariance property. In this study, we present the results of potential multiple scalings in the long-term heart rate data from young healthy adults subjected to normal daily activity. Our approach is based on the direct check of the probabilistic structure of the increment process. Results from fractional Brownian motion are compared and the generating mechanism for multiple scaling is discussed in the context of scale-invariance formalism.

Keywords: scale invariance, multiple scaling, heart rate variability

1   Introduction

Many physical processes are scale invariant, giving rise to renormalizable structure and self-similarity in space and time. It is quite often that the renormalization can be conducted at different scales with different scaling exponents, namely, a multiple scaling property. Multiple scaling was observed in many natural phenomena ranging from physical[1,2,3,4,5,6], biological[7,8,9,10], to economical systems[1,11,12]. When a multiplicative mechanism is involved in the dynamics, *multifractal* theory can be used to characterize a (continuous) set of singularity exponents and the (Hausdorff) dimension of their supports via a Legendre transformation. Successful applications of the formalism revealed deep insights about many natural processes such as the density profile in diffusion limited aggregates[13,14], the velocity and dissipation fields in fully developed turbulence[15,2,3], the money exchange index from financial market[1,11,12] and network traffic[5,6]. In general, there is not an unified theory for multiple scaling and, sometimes, only finite number of scaling exponents can be ascertained. In this work, we will present such an example in the long-term heart rate variability (HRV) from healthy young adults and discuss its generating mechanism.

The study of HRV has continued to draw great interests in recent years. It is of both fundamental and clinical importance. In particular, a "healthy" heart typ-

ically shows a power-law like power spectrum[16], which can imply scale invariance[a] and "self-similarity" in the autonomous nervous system. Losing such variability was found to correlate well with the mortality rate of heart diseased patients[17]. The variation in the HRV scaling has been discussed by a number of researchers in the past[7,8,10]. In particular, Peng et. al. developed the systematic method and compared the power-law scalings in the very short time scale (a few heart beats) with the "asymptotic" behaviour (above 1000 heart beats). Significant difference was concluded in these widely separated time scales and the characteristic was found sufficient to distinguish between the healthy subjects and patients with congestive heart failure[10]. Di Rienzo et. al. also noted the variation of the power-law exponent of HRV in frequency, which in turns causes variations of the power-law scaling of the blood pressure as well[7]. Later, Viswanathan et. al. tackled the non-uniformity of power law scaling between the healthy subjects and those with severe heart disease from a point-process aspect[18]. Again, the conclusion was drawn on the distinguishability between the health and disease. In these previous studies, multiple scaling within physiologically relevant range of healthy humans has not been explored.

In this work, multiple scaling was studied based on the data increment process. The increment process at various time lags enables us to focus on the *local scale invariance* property of the data. The numerical method was developed and tested on artificial time series with one- and multiple- scaling exponents and then applied to the heart rate data set. We also compared with the existing methodology in the literature and found noticeable difference in the result. This paper is organized as follows. The main ideas and the numerical method are introduced in the next section. The results of artificial time series and the evidence of multiple scaling in heart rate data are presented in section 3. In the last section, the mechanism generating the multiple scaling in HRV will be discussed in the context of scale invariance formalism.

2 Extract Scale Invariance from the Probability Density Function

In this section, we will first recall the basic definition of scale invariance of a process and then describe the numerical method to extract multiple scaling. Given a time series, $\mathbf{r}(s)$, its scale invariance is defined by the family of probability density functions of the increment, $\Delta\mathbf{r}(t;s) = \mathbf{r}(t+s) - \mathbf{r}(s)$: for any λ and a fixed constant h, one has

$$f_{\lambda t}(n) = \lambda^{-h} f_t(\lambda^{-h} n) \tag{1}$$

where f_t denotes the probability density function of $n \equiv \Delta\mathbf{r}(t;s)$ and the constant h is the scaling index or scaling exponent of $\mathbf{r}(s)$.

To study (1) numerically requires the assumption of stationarity. This appears to hold in our application. When the increment is stationary, $f_t(n)$ can then be estimated from the ensemble of $\{\Delta\mathbf{r}(t;s), s = 1, 2, \cdots\}$. Due to the data fluctuation, it was found more efficient to fit $f_t(n)$ with a specific form, say $g_t(n)$, than

---

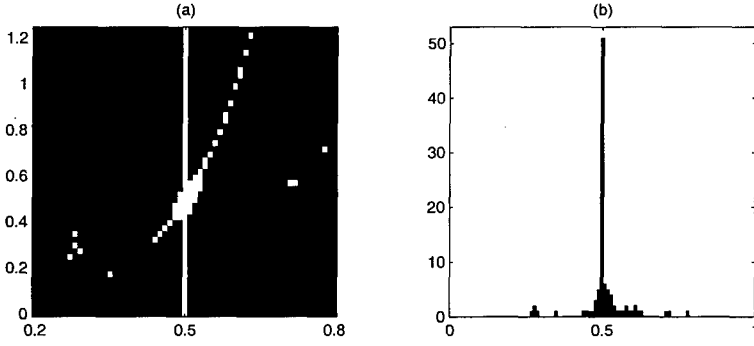[a]Note that power-law spectrum is only a necessary condition[19,20].

Figure 1. (a) The set $\mathcal{N}(\mathbf{T}; h)$ plotted on the $h - n$ plane for $\mathbf{T} = \{2^k, \ k = 0, 1, 2, 3\}$ and $h_o = 0.5$, dark pixels: $|\mathcal{N}| = 0$, white pixels: $|\mathcal{N}| > 0$, (b) $\mu(\mathbf{T}; h)$ vs. h plot. The family of density functions used in this demonstration was ideal in that they have the Gaussian form: $\{g_t(n) = \exp(-n^2/2\sigma(t)^2)/\sqrt{2\pi\sigma(t)^2}, \sigma(t) = \sqrt{t}; \ t = 2^k, k = 0, \cdots 11\}$.

working directly with the histogram of $\Delta \mathbf{r}(t)$ in (1). For example, for the fractional Brownian motion, a Gaussian form is assumed for $g_t(n)$. In this case, the maximum likelihood method was used to minimize the likelihood function $-\log(\Pi_i g_t(n_i))$ in order to extract the mean and variance of a Gaussian probability density function. This approach is subjected to less bias comparing to, say, minimizing the L^2 norm between the histogram and $g_t(n)^{21}$. After $g_t(n)$ is defined, (1) can be studied by systematically varying n, λ and h_o values. Let

$$u(n, \lambda; h) = \frac{f_{\lambda t}(n)}{f_t(\lambda^{-h} n)}. \tag{2}$$

and denote the estimated slope, $d\log(u)/d\log(\lambda)$, as h'. $\mathbf{r}$ is said to be renormalizable or is scale invariant with a scaling exponent h_o if $h' \sim h_o$.

The parameters used in the numerical experiment were $t = 1$, $\lambda \in \{2^k, k = 0, \cdots, 11\}$ and $h \in \{0.01 \cdot k, \ k = 0, \cdots, 100\}$. The estimated slope h' is in general a function of n, h, and λ. The range of λ in which h' is estimated reveals the time scale of the local scale invariance property of $\mathbf{r}(s)$. Once the parameters are defined, we first construct, for a given h, $\mathcal{N}(\mathbf{T}; h) = \{n, \ |h'(n, \lambda; h) - h| < \epsilon\}$ with $\epsilon = 0.01$ to keep the error between h' and h less less than 1%. Here, $\mathbf{T}$ denotes the set of λ's where the condition $|h' - h| < \epsilon$ is satisfied. For any given h and $\mathbf{T}$, $\mathcal{N}$ contains the set of n's in which local scale invariance is defined. The scaling interval of h' can thus be calculated by the logarithm of the ratio of the largest and smallest λ in $\mathbf{T}$. For each h, (1) also contains an isolated solution (when the set $\mathcal{N}$ has only one element) which has no relevance in the current context (Fig. 1a). Fortunately, these isolated solutions form a small set. Hence, given any $\mathbf{T}$ and h, $\mu(\mathbf{T}; h) = |\mathcal{N}(\mathbf{T}; h)|$, where $|\cdot|$ returns the number of elements at a specific h value, will show a peak at the desired scaling exponent (Fig. 1b).
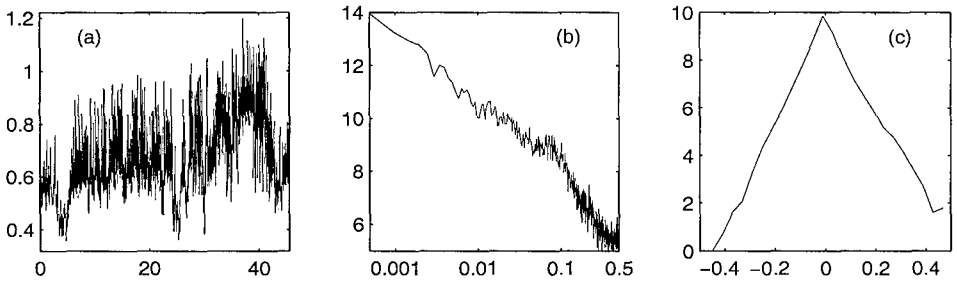
Figure 2. (a) Typical RR-interval record ($r(s)$ (sec) vs. s ($\times 10^3$ beat)), (b) the power spectral density function of $r(s)$ (in log-log scale). (c) histogram of $\Delta r(t), t = 4$ (in linear-log scale).

3   Numerical Evidence of Multiple Scaling in HRV

3.1   Experimental Procedure

Six young adults (average age: 25 yr, height: 173 cm, weight: 74 kg) participated in the experiment. The subjects were allowed to conduct their normal daily activity. The difference in the body surface potential was sampled at 1000 Hz for a period of approximately 24 hours. The data was then down-loaded to a PC and a specialized computer code was written to search for the QRS complex for each heart beat with proper filtering for events such as skip-beat, PVC, and so on. The time span between the successive contractions of the ventricles, measured as the RR-interval (RRi), was finally extracted and used in the scale invariance analysis.

A representative day-time RRi data is shown in Fig. 2a. Scale invariance in the RRi data may be implied by the power-law trend of the power spectrum (Fig. 2b). But it is clear that a single power-law is not sufficient to describe the spectrum over the full frequency range.

3.2   Numerical Results

Before applying the numerical method to the RRi data, we first tested it on the fractional Brownian motion of scaling exponent $h_o = 0.26, 0.5, 0.78$. Each artificial time series had 40,000 samples and was generated by using the spectral method[19,20]. Fig. 3a shows a typical case of the set $\mathcal{N}$ plotted on the $h - T$ plane where $T = 2^k, k = 1, 2, \cdots$ Sometimes, it is useful to consider $\sum \mu(T; h)$ over all T sets for a given h. The result is shown in Fig. 3b where the scaling exponent is indicated at the location of the peak. It is clear that the desired scaling exponents were captured with good accuracy.

We next apply the spectral method to construct a two-exponent artificial time series of 2^{16} data points (Fig. 4a). The local scale invariance in the time series was defined by the scaling exponent $h_o = 0.26$ for frequency below 0.0025Hz and $h_o = 0.78$ above 0.0025Hz. Fig. 4d was plotted with $\sum \mu(T; h)$ versus h and the estimated $h's$ were within 3% of the exact values. In Fig. 4c, we checked the minimum time scale of the exponents, which is defined by the smallest element of
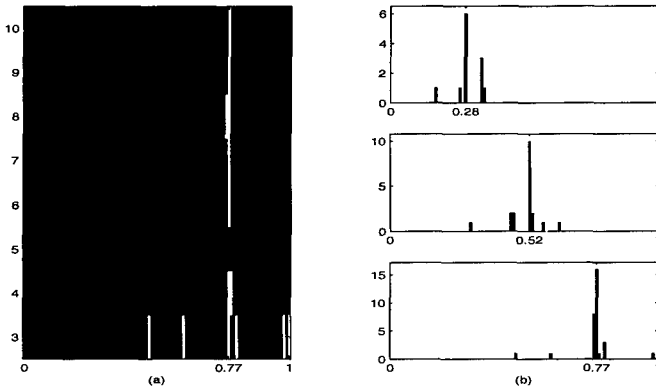
Figure 3. (a) The set μ on the $h - \mathbf{T}$ plane, dark pixels: $|\mu| = 0$, white pixels: $|\mu| > 0$ for $h_o = 0.78$. (b) $\sum \mu(\mathbf{T}; h)$ vs. h for $h_o = 0.26, 0.5, 0.78$.

the $\mathbf{T}$ set. This is obtained by constructing the set $\eta(T; h)$ where T is the smallest λ in the corresponding $\mathbf{T}$ set. The set η shown on the $h - \log_2(T)$ plane reveals the minimum time scale from which the exponent is defined (Fig. 4c). For the artificial time series, it was found that correct time scales of the exponent were captured: i.e., the "fast" dynamics (above 0.0025Hz) of $h_o = 0.78$ prevails in small λ's and the "slow" dynamics of $h_o = 0.26$ at large λ (see Fig. 4c caption).

To study the RRi data, the following form of probability density function was assumed (based on Fig. 1c):

$$g_t(n) = \frac{\exp(-|n|^\alpha/t^\beta)}{\gamma}. \tag{4}$$

The RRi data of all the test subjects exhibit multiple scaling characteristics. In what follows, we will present the evidence from a typical individual whose data has been given in Fig. 2. In Fig. 5a, multiple peaks were seen from the $\sum \mu$ vs. h plot, indicating multiple scaling of HRV. At least five "significant" exponents were identified ($a \sim e$ in Fig. 5a). The minimum time scale of these exponents scattered over the range of $\lambda = 2^1$ to 2^8 (Fig. 5b). The inverse of this range covers the "frequency" < 0.0039 (1/beat) to 0.5 (1/beat) in the power spectrum (Fig. 2b). In this range, two linear regions of slopes $\zeta \sim -1.4$ and -2.1 may be roughly defined. Based on $\zeta = 1 + 2h$, they match nicely to two of the peak locations $h = 0.17$ and 0.6 in Fig. 5a. The size of the scaling interval is shown by the set $\mathcal{N}$ plotted on the $h - |\mathbf{T}|$ plane (Fig. 5c). A wide range of scaling interval associated with the scaling exponents found in Fig. 5a is again seen.

Finally, we compared our method with the *detrend fluctuation analysis* (DFA)[8,10] and found noticeable difference. In Fig. 6 shows the double-logarithmic plot of the average variance versus the scaled window length. Only one exponent can be ascertained here since the local scale invariance characteristics have been averaged out in the process of DFA.
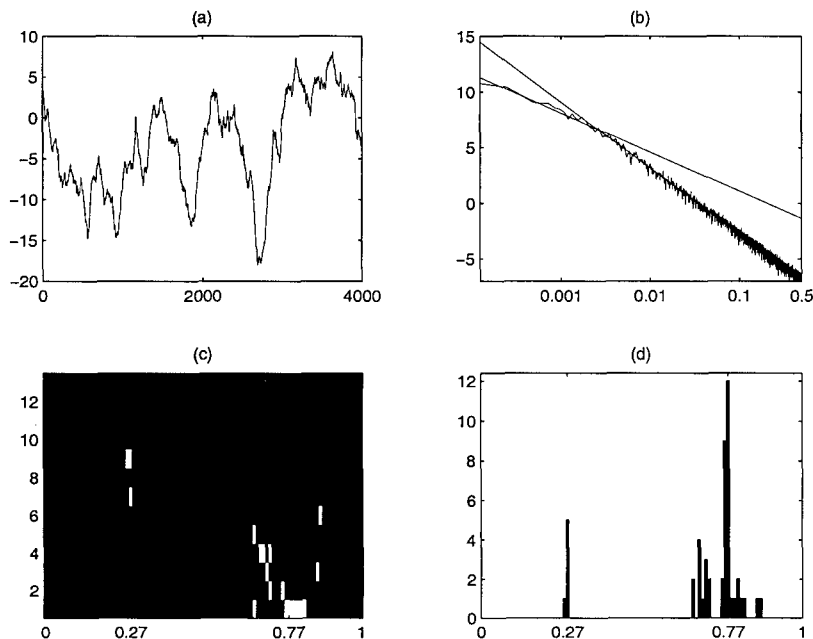
Figure 4. (a) Two-time-scale artificial time series, (b) power spectral density of the time series: the scaling exponents are $h_o = 0.26$ for $f < 0.0025Hz$ and $h_o = 0.78$ for $f > 0.0025Hz$. (Note: $0.0025 = 2^{-8.6}$). The line segments have slops of -1.52 and -2.56, respectively. (c) The set η plotted on $h - \log_2(T)$ plane, dark pixels: $|\eta| = 0$, white pixels: $|\eta| > 0$. The scaling range for $h = 0.77$ was captured for $T < 2^7$ and that for $h = 0.27$ for $T = 2^7 \sim 2^9$. (d) $\sum \mu(\mathbf{T}; h)$ vs. h plot.
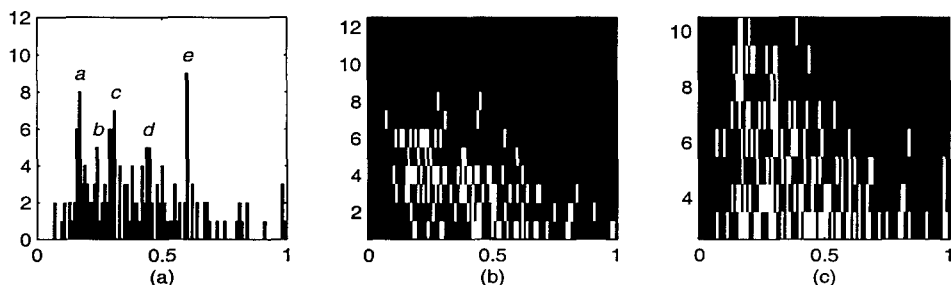

Figure 5. (a) $\sum \mu(\mathbf{T}; h)$ vs. h plot. Identified peaks at h=0.17, 0.24, 0.31, 0.44, 0.6 are labeled as a, b, c, d, e, respectively; (b) the set η plotted on $h - \log(T)$ plane, dark pixels: $|\eta| = 0$ and white pixels: $|\eta| > 0$, (c) The set of $\mathcal{N}$ plotted on $h - \log_2(T)$ plane, dark pixels: $|\mathcal{N}| = 0$, white pixels: $|\mathcal{N}| > 0$.

4   Discussion and Future Outlook

Numerical evidence of multiple scaling of HRV in physiologically relevant range has been presented for the case of healthy young adults. The scale invariance was
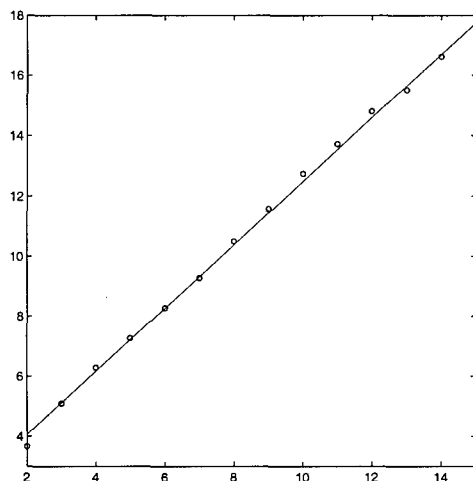
Figure 6. Detrend fluctuation analysis on the RRi data shown in Fig. 2a: averaged variance of the detrend time series vs. window length plot on double logarithmic scales (symbol: 'o'). The fitted line of slope ~ 1.05, suggesting $h = 0.05$, was shown as the solid line.

extracted based on the property of the family of RRi increment probability density functions. This approach enables us to explore local scale invariance property in the data. Although it is only a bit costlier in computation, details previously unavailable from other global methods, such as the power spectral density function or DFA, may be obtained. It should be noted that the current methodology is not able to extract temporal structure of very short duration. When such a rare event occurs, its characteristics will yield to that generated by the more "regular" dynamics in the process of estimating the density function. What this work has shown is that even the "regular" neuro-control of our cardiovascular system is rich enough to encompass a wide range of time scales and scaling structures, i.e., multiple scaling. Indeed, the process is very complex, as Hausdorff and Peng showed from artificial time series that the "balance" of different inputs to the system is also crucial to generate the 1/f scaling[8].

More detailed characterization of the density function (4) is underway and will provide the insight of the generating mechanism of multiple scaling. For example, the variation of the parameters α, β and γ in (4) can imply self-similarity of the individual density function at specific time lag (λt). This in turns can lead to scale invariant solution of (1) over finite n-interval. In particular, given a $\Delta \in \mathbf{R}$ and $n' \in I_n(\lambda t)$, assume the graph $f_{\lambda t}(n)$ is self-similar in the interval I_n:

$$\lambda^\Delta f_{\lambda t}(\lambda^\Delta n') = f_{\lambda t}(n'). \tag{5}$$

Since it can be written

$$f_{\lambda t}(n') = f_{\lambda t}(\lambda^h n''), \tag{6}$$

(5) implies

$$\lambda^\Delta f_{\lambda t}(\lambda^\Delta n') = \lambda^{-h} f_t(n'') \tag{7}$$

where $n' = \lambda^h n''$. Re-arranging terms in (7), one finds

$$\lambda^{h+\Delta} f_{\lambda t}(\lambda^{h+\Delta} n'') = f_t(n'') \tag{8}$$

which is of the same form as (1). Hence, (8) implies the existence of a new exponent $h + \Delta$. Substituting the newly found exponent into the scale invariance formalism (1), even more can be revealed by following the same arguments. In general, we found, when certain conditions are met, the number of exponents can "grow" as a power-law by repeating (5) with all the exponents. However, the scaling interval I_n also shrinks at the same time by a power-law, making most of the exponents "unobservable[22]" . We will report more details in a future publication.

Acknowledgments

References

1. A. Hilgers and C. Beck, *Int. J. Bif. & Chaos* **7**, 1855 (1997).
2. V.S. L'vov and I. Procaccia, *Phys. Rev. Lett.* **76**, 3963 (1996); *Phys. Rev. Lett.* **77**, 3541 (1996); *Phys. Rev.* E **54**, 6268 (1996).
3. B.B. Mandelbrot, *J. Fluid Mech.* **62**, 331 (1974).
4. Y. Pesin and H. Weiss, *J. Stat. Phys.* **86**, 233 (1997).
5. R.H. Riedi, M.S. Crouse, V.J. Ribeiro and R.G. Baraniuk, *IEEE. Trans. Info. on Theo.* **45**, 992 (1999).
6. J.M. Tchéou, M.E. Brachet, F. Belin, P. Tabeling and H. Willaime, *Physica* D **129**, 93 (1999).
7. M. Di Rienzo, G. Parati, A. Pedotti and P. Castiglioni, *Frontiers of Blood Pressure and Heart Rate Analysis*, Ed. M. Di Rienzo, G. Mancia, G. Parati, A. Pedotti and A. Zanchetti (IOS Press, 1997).
8. J.M. Hausdorff and C.-K. Peng, *Phys. Rev.* E **54**, 2154 (1996).
9. D.C. Lin and K Behdinan, *Proc. 1st Canadian Conference on Nonlinear Solid Mechanics*, **2**, 589 (1999).
10. C.K. Peng, S. Havlin, H.E. Stanley and A.L. Goldberger, *Chaos, Soliton & Fractal* **5**, 82 (1995).
11. B.B. Mandelbrot, A. Fisher and L. Calvet, *Cowles Foundation*, Paper No. 1164 (1997).
12. A. Fisher, L. Calvet and B.B. Mandelbrot, *Cowles Foundation*, Paper No. 1166 (1997), http://www.econ.yale.edu/ fisher/papers.html
13. C. Amitrano, A. Coniglio, P. Meakin and M. Zannetti, PRB **44**, 4974 (1991).
14. A. Coniglio, *Physica* A **140**, 51 (1986).
15. U. Frisch, *Turbulence: The Legacy of A.N. Kolmogorov* (Camb. Press. 1995).
16. M. Kobayashi and T. Musha, *IEEE. Trans. on Biomed. Eng.* **29**, 456 (1982).
17. J.T. Bigger Jr., J.L. Fleiss, R.C. Steinman, L.M. Rolnitzky, R.E. Kleiger and J.N. Rottman, *Circulation* **85**, 164 (1992).

18. G.M. Viswanathan, C.-K. Peng, H.E. Stanley and A.L. Goldberger, *Phys. Rev. E* **55**, 845 (1997).
19. N.P. Greis and H.S. Greenside, *Phys. Rev.* A **44**, 2324 (1991).
20. T. Highchi, *Physica* D **31**, 277 (1988); *Physica* D **46**, 254 (1990).
21. S. Mercik and R. Weron, *Physica* A **267**, 239 (1999).
22. D.C. Lin and R.L. Hughson, in preparation.